Experimental investigation of opacity models for stellar interior, inertial fusion, and high energy density plasmas[a)]

J. E. Bailey,[1,b)] G. A. Rochau,[1] R. C. Mancini,[2] C. A. Iglesias,[3] J. J. MacFarlane,[4] I. E. Golovkin,[4] C. Blancard,[5] Ph. Cosse,[5] and G. Faussurier[5]
[1]*Sandia National Laboratories, Albuquerque, New Mexico, 87185-1196, USA*
[2]*University of Nevada, Reno, Nevada 89557, USA*
[3]*Lawrence Livermore National Laboratory, University of California, Livermore, California 94550, USA*
[4]*Prism Computational Sciences, Madison, Wisconsin 53703, USA*
[5]*CEA, DAM, DIF, F-91297 Arpajon, France*

(Received 7 December 2008; accepted 15 December 2008; published online 23 March 2009)

Theoretical opacities are required for calculating energy transport in plasmas. In particular, understanding stellar interiors, inertial fusion, and Z pinches depends on the opacities of mid-atomic-number elements over a wide range of temperatures. The 150–300 eV temperature range is particularly interesting. The opacity models are complex and experimental validation is crucial. For example, solar models presently disagree with helioseismology and one possible explanation is inadequate theoretical opacities. Testing these opacities requires well-characterized plasmas at temperatures high enough to produce the ion charge states that exist in the sun. Typical opacity experiments heat a sample using x rays and measure the spectrally resolved transmission with a backlight. The difficulty grows as the temperature increases because the heating x-ray source must supply more energy and the backlight must be bright enough to overwhelm the plasma self-emission. These problems can be overcome with the new generation of high energy density (HED) facilities. For example, recent experiments at Sandia's Z facility [M. K. Matzen *et al.*, Phys. Plasmas **12**, 055503 (2005)] measured the transmission of a mixed Mg and Fe plasma heated to 156 ± 6 eV. This capability will also advance opacity science for other HED plasmas. This tutorial reviews experimental methods for testing opacity models, including experiment design, transmission measurement methods, accuracy evaluation, and plasma diagnostics. The solar interior serves as a focal problem and Z facility experiments illustrate the techniques. © *2009 American Institute of Physics*. [DOI: 10.1063/1.3089604]

I. INTRODUCTION

Physical pictures for high energy density (HED) plasmas rely on models of the plasma properties. For example, the inner structure of astrophysical plasmas such as stars is often inaccessible to direct measurements. In his seminal book "The internal constitution of the stars" Eddington[1] pointed out this dilemma, but goes on to show that we can still build physical pictures for the inner workings of a star as long as we know the properties of the matter that lies within. More detailed information may be available for laboratory plasmas such as inertial fusion implosions and Z pinches. However, building a complete physical description still normally requires material property models.

Radiation often plays an essential role in both astrophysical and laboratory HED plasmas and a key material property is the *opacity*, which quantifies how transparent or opaque the plasma is to radiation. In this tutorial we describe experimental methods developed to test opacity models for HED plasmas.

The transmission of photons with intensity I_0 normally incident on a uniform plasma is given by

$$T(\nu) = I(\nu)/I_0(\nu) = \exp - \tau(\nu), \tag{1}$$

where $h\nu$ is the photon energy and $I(\nu)$ is the attenuated photon intensity emerging from the plasma. The optical depth, $\tau(\nu)$, is related to the opacity by $\tau(\nu) = \kappa(\nu)\rho x$, where $\kappa(\nu)$ is the opacity per unit mass (typically measured in units of cm^2/g), ρ is the density, and x is the optical path length. Opacity models are tested by measuring $T(\nu)$ through a plasma with known characteristics.

The opacity is generally a rapidly varying function of frequency. In some applications, knowledge of the frequency dependent opacity is required and this is what must be measured in benchmark experiments. An example is levitation of "metals" in stellar interiors.[2] Here, metals refer to any element other than hydrogen or helium, a definition commonly employed in astrophysics. These elements diffuse toward the center of stars under the influence of gravity. There is an opposing levitating force provided by the photon pressure and this force is proportional to the frequency dependent opacity.

In other applications the most important quantity is the mean opacity averaged over frequency. An example is diffusive radiation transport of energy within stellar interiors.[3] In light of this simplification, one might ask: Why use opacity models? Why not just measure the mean opacities we require? The problem is that the opacity depends on the plasma

[a)]Paper PT2 1, Bull. Am. Phys. Soc. **53**, 199 (2008).
[b)]Invited speaker.

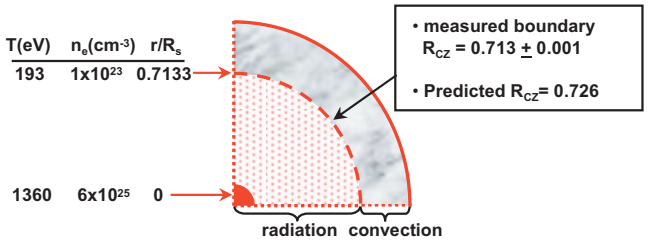

FIG. 1. (Color) Schematic of the solar interior. The temperature and density information are from Ref. 4 and the values for the location of the radiation convection boundary are from Ref. 5.

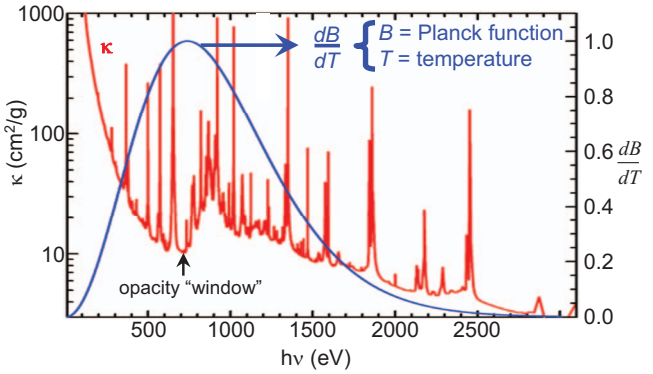

FIG. 2. (Color) Frequency dependent opacity (Refs. 13 and 14) for a 17 element solar composition (Ref. 6) near the base of the solar convection zone compared to dB/dT. The electron temperature and density were 193 eV and 1×10^{23} cm^{-3}, respectively.

temperature, density, and elemental composition. The breadth of plasma conditions and constituents encountered in applications makes it impractical to measure all the needed opacities. Furthermore, accurate opacity measurements are challenging and the number of available measurements is sparse. Finally, some interesting conditions remain beyond the reach of laboratory experiments. Therefore, the main goal of opacity experiments is to test the physical underpinnings of opacity models so that they can be reliably extrapolated to conditions untested in the laboratory. Fortunately, the details of the rapidly varying opacity as a function of frequency provide a trove of information. The accuracy of model descriptions for the physical processes that govern opacity is severely tested by comparison with $T(v)$ measurements.

II. OPACITY EXPERIMENT DESIGN

Given that opacity measurements are sparse and the parameter space is broad, it is important to optimize opacity experiment designs. The questions we must answer include the following.

(1) What photon energy range is important?
(2) What elements contribute?
(3) What photon absorption processes are important?

The answers to these questions depend on the application.

In this tutorial we use the solar interior as an example to illustrate experiment design and execution. Figure 1 provides a schematic of the solar interior. The energy generated by thermonuclear reactions in the solar core is transported outward by radiation over approximately 70% of the solar radius, R_s. The solar opacity generally increases with radius and eventually becomes large enough that energy transport by radiation is inefficient and convective transport takes over. The border between the radiation and convection dominated zones is known as the CZ boundary. The core temperature is roughly 1360 eV and it falls to approximately 190 eV just below the CZ boundary.[4] The electron density also decreases, from 6×10^{25} cm^{-3} at the core to 1×10^{23} cm^{-3} near the CZ boundary. The boundary location is $R/R_s=0.713\pm0.001$, inferred with remarkable accuracy from helioseismology measurements.[5] The CZ boundary location and the spatial temperature and density profiles depend on the mean opacity as a function of radius. However, opacity models have never been tested with laboratory experiments at the conditions that exist inside the sun.

The motivation for experimental verification of theoretical opacities has grown sharper during the past decade. Solar models are constructed using estimates for the composition and the material properties such as equation of state, opacity, and nuclear cross sections as inputs. Predictions for the CZ boundary location, interior density profile, and sound speed were in good agreement with helioseismic data until roughly the year 2000. Beginning in 1999, revised estimates for the solar composition reduced the amount of metals.[6] Solar models based on these revised estimates disagree with helioseismology.[5,7,8] One possible explanation is inaccuracies in the opacity models. Solar models constructed with *ad hoc* adjustments of the opacity[5,7,9,10] found that increasing the mean opacity by 10%–20% in the solar region $0.4<R/R_s<0.7$ would resolve the discrepancies.

The solar problem serves to define needed opacity experiments. The first question to answer is what photon energy range is most important. For plasmas such as the sun that are much larger than the photon mean free path, radiation transport is usually described by a diffusion approximation[11,12] using the Rosseland mean opacity κ_R,

$$\frac{1}{\kappa_R}=\int d\nu\frac{1}{\kappa(\nu)}\frac{dB}{dT}\Big/\int d\nu\frac{dB}{dT}, \tag{2}$$

where B is the Planck function, T is the plasma temperature, and the weighting function dB/dT peaks at roughly 3.8 kT. Note that the Rosseland opacity is a harmonic mean depending on the reciprocal of $\kappa(\nu)$ and photons are most efficiently transported through the "windows" where $\kappa(\nu)$ is the lowest. Near the CZ boundary $T\sim190$ eV and dB/dT peaks at $h\nu\sim750$ eV (Fig. 2). The frequency dependent opacity near the CZ boundary calculated using the opacity project model[13,14] is displayed in Fig. 2. Comparison with the weighting function for the Rosseland mean shows that the most important photon energies are approximately $300<h\nu<1300$ eV. We reiterate that we require measurements of the frequency dependent opacity to test the physics in opacity models. However, familiarity with the characteristics of the Rosseland mean helps define what opacities are most important to measure.

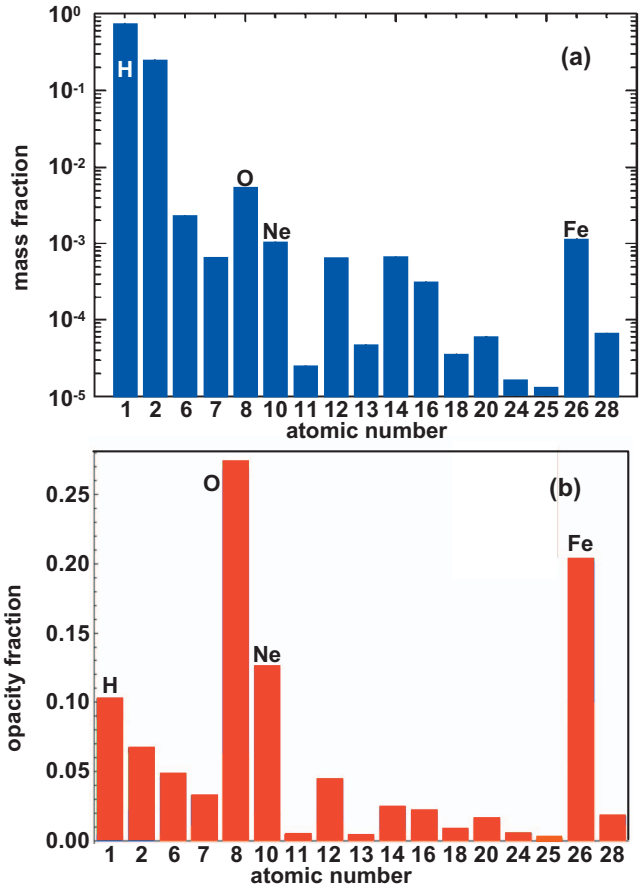

FIG. 3. (Color) Characteristics of the solar interior composition. The histogram in a provides the mass fractions (Ref. 16). The histogram in b is the fractional contribution to the Rosseland mean evaluated near the base of the solar convection zone using the OPAS opacity model (Ref. 17).

The second question to answer in designing opacity experiments is: What elements should be studied? The answer is sometimes straightforward in laboratory plasmas composed of a single element. However, in many applications multielement plasmas are used. For example, mixtures of low-Z and mid-Z elements, where Z is the atomic number, are commonly used in inertial fusion capsule ablators (Be/Cu ablators are described in Ref. 15). Different elements may be present in different plasma spatial regions. These differences may alter the opacity and the role each element plays in the radiation transport.

Astrophysical plasmas are more complicated since the observer does not necessarily possess certain knowledge of the composition and many elements may be present. The solar composition estimated from photospheric spectroscopy and meteorite analysis[16] is illustrated in Fig. 3(a). This 17-element mixture was widely used prior to the revised low-metallicity estimates[6] that led to the solar CZ problem.[5] The mass fraction for elements such as oxygen, neon, and iron is less than 1%. Nevertheless, these elements contribute a disproportionately large fraction of the solar interior opacity because they are not completely ionized, as described below. The fractional opacity contribution for each element at conditions corresponding to the CZ boundary is shown in Fig. 3(b). Figure 3(b) calculations were performed with the OPAS model.[17] The largest contributions are from oxygen, neon, and iron and these are the elements of greatest interest for solar interior opacity measurements.[5] Obviously, the impact of errors in any single element is diminished when the element is a dilute constituent of a mixture. For example, in order to cause a 10% change in the total mean opacity we would need to multiply the iron opacity at the CZ boundary by a factor of approximately 1.5.

The third question for opacity experiment design is how each element contributes. The three main absorption processes in plasmas are free-free, bound-free, and bound-bound electron transitions. These processes differ from one element to another and depend on the ionization. Consider the contributions of hydrogen, oxygen, and iron to the opacity at the base of the solar convection zone. At these conditions hydrogen is fully stripped and the only contribution is free-free transitions in the ionized electrons [Fig. 4(a)]. Oxygen is ionized into the K-shell (i.e., O^{+6} and O^{+7}, isoelectronic with He and H) and contributes absorption through both bound-free and bound-bound transitions. Here, "K-shell" refers to $n=1$ principal quantum number electron states. K-shell ions in local thermodynamic equilibrium (LTE) normally have much of their population in the ground state and an important class of transitions originates from the $n=1$ lower level [Fig. 4(b)]. At the CZ boundary, iron is ionized into the L-shell, with significant populations of Fe^{+16}, Fe^{+17}, and Fe^{+18}. These ions are isoelectronic with Ne, F, and O and consequently are often described as Ne-like, F-like, and O-like. The greater number of bound electrons renders the Fe opacity contributions immensely complicated. Many transitions originate from the $n=2$ lower level, but there is also significant excited state population and transitions originate from $n \geq 3$ principal quantum numbers [Fig. 4(c)]. Of the three elements that are most important at the CZ boundary, Fe is by far the most complex and it is therefore expected to be the most suspect.

The opacity plots in Figs. 4(b) and 4(c) illustrate another consequence of mixing elements together. Consider the pure iron photon absorption [red curve, Fig. 4(c)]. The deepest opacity window is in the vicinity of $h\nu \sim 500-700$ eV, a region dominated by bound-free transitions with excited initial states. If one is interested in a pure iron plasma, then this defines the most important photon energy range. The opacity model must then have an accurate treatment for both the $n \geq 3$ excited state populations and the bound-free photoionization cross sections out of those excited states. On the other hand, the comparison of pure iron opacity with the total solar mixture opacity shows that the iron contribution to the $h\nu \sim 500$ eV photon energy range is negligible. The mixture opacity has filled in the Fe window at these energies. Instead, the Fe bound-bound transitions at $750 < h\nu < 1300$ eV are the most significant iron contribution to the solar mixture opacity near the CZ base. Thus, a mixture dilutes the importance of any individual element and can change which absorption processes and photon energies are important.

These considerations define a useful opacity experiment for the base of the solar convection zone. We should attempt to measure opacities for O, Ne, and Fe. Of these, Fe is probably the most suspect and is therefore a good place to start.

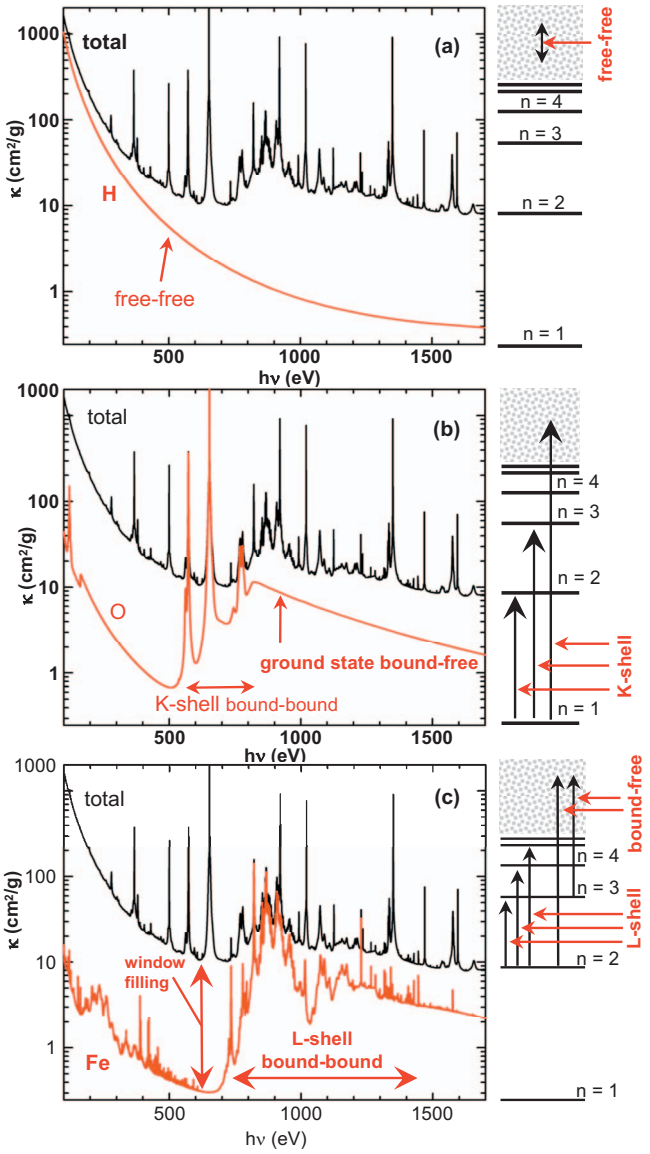

FIG. 4. (Color) Physical processes responsible for the contribution to opacity by different elements. The calculated (Refs. 13 and 14) total opacity of the solar mixture at the base of the convection zone is compared with the contribution from hydrogen, oxygen, and iron in (a), (b), and (c), respectively.

The most important photon energy range for Fe was already established as 750–1350 eV. The electron temperature just below the convection zone is ~190 eV and the electron density is 10^{23} cm^{-3}. Eventually we must reproduce these conditions in order to test fully the model physics. This is a daunting goal that is beyond the ability of present day experiments. However, the ionization distribution depends on both temperature and density, a property that enables progress while experimental techniques to reach more extreme conditions are developed.

Reproducing the charge states of interest is a key prerequisite for quantitative tests of opacities. It can determine whether opacity models accurately calculate the charge state distribution, energy level structure, and relevant photon absorption processes. Calculations[18] of iron charge state distributions at various depths within the sun are shown in Fig. 5.

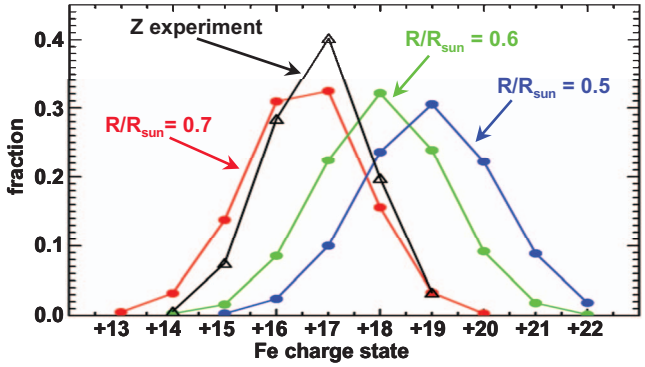

FIG. 5. (Color) The iron charge state distribution as a function of electron temperature and density at different depths within the sun. The T_e and n_e values are from Ref. 4 and the PrismSPECT model (Ref. 18) was used to calculate the charge state distribution. The red curve corresponds to just below the convection zone (R/R_s=0.7, T_e=193 eV, $n_e=1\times10^{23}$ cm^{-3}), the green curve corresponds to R/R_s=0.6 (T_e=261 eV, $n_e=2.5\times10^{23}$ cm^{-3}), and the blue curve corresponds to R/R_s=0.5 (T_e=335 eV, $n_e=7\times10^{23}$ cm^{-3}). The black curve with triangles corresponds to the distribution for conditions in Z experiments.

Deeper in the solar interior both the temperature and density increase. Although the temperature rise should cause a higher degree of ionization, it is countered by the corresponding density increase. Thus, similar iron charge states exist over a broad range of the solar interior. The conditions corresponding to recent Z facility iron experiments[19,20] are superimposed on the solar interior results in Fig. 5. The Z facility experiment charge state distribution is similar to those at the CZ boundary, even though the 156 eV Z experiment temperature is ~37 eV lower. The reason is that the density is approximately ten times lower. Tests of high density effects such as continuum lowering and line broadening require further experiment advances to simultaneously produce both high temperature and density.

III. EXPERIMENTAL METHODS AND HISTORICAL OVERVIEW

The basic strategy used to test opacity models is to compare the frequency dependent experimental and theoretical transmission for a sample with known conditions. This method is illustrated in Fig. 6. The sample is heated with an x-ray source and the transmission is measured by viewing a backlight through the sample with a spectrometer. The sample material of interest is sandwiched by layers of a low-Z tamper to promote uniformity. Spectra are acquired with and without the sample material. Dividing the absorption spectrum obtained with the sample by the unattenuated (tamper only) spectrum provides the transmission.

The requisite data can be acquired on separate experiments, as long as key experimental aspects are reproducible. Reproducibility can be evaluated by comparing spectra obtained on sequential experiments (Fig. 7). The reproducibility encompasses the x-ray heating of the sample, the sample fabrication, the backlight absolute intensity and spectrum, the spectrometer efficiency (e.g., crystal reflectivity) and the detector response (e.g., film processing reproducibility). A powerful alternative method known as point projection

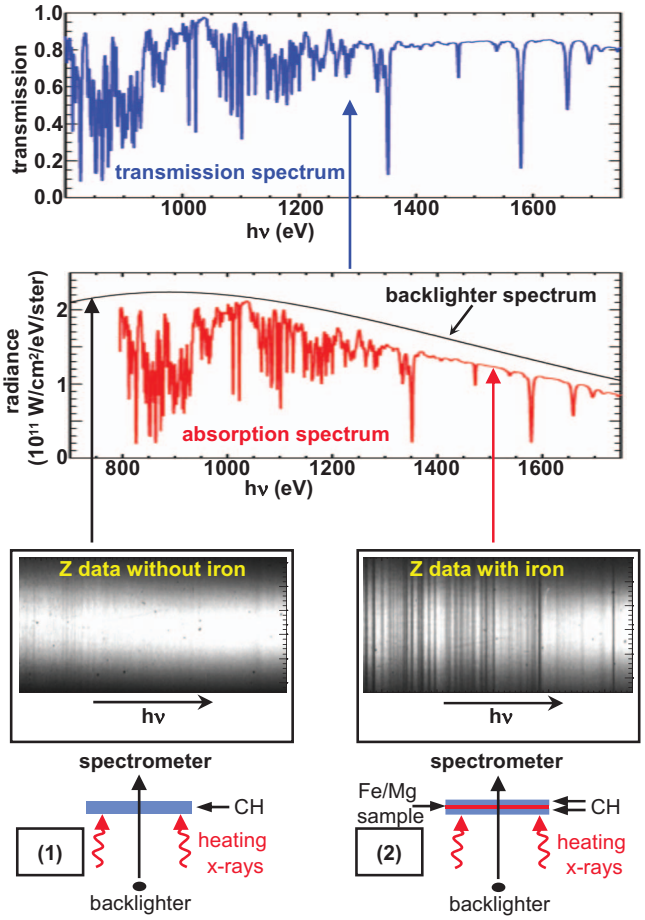

FIG. 6. (Color) Method for transmission measurements used to test opacity models. A spectrometer views a backlight through an x-ray heated foil. The sample transmission as a function of photon energy is determined using measurements of a low-Z tamper only foil (diagram 1) and measurements of the sample material of interest surrounded by the tamper (diagram 2). The synthetic backlighter spectrum is a 314 eV Planckian that is representative of the backlighter used in *Z* iron experiments (Refs. 19 and 20). The absorption spectrum was calculated with PrismSPECT (Ref. 18) at the experiment temperature and density values and the transmission spectrum was obtained by dividing the absorption spectrum by the backlighter spectrum.

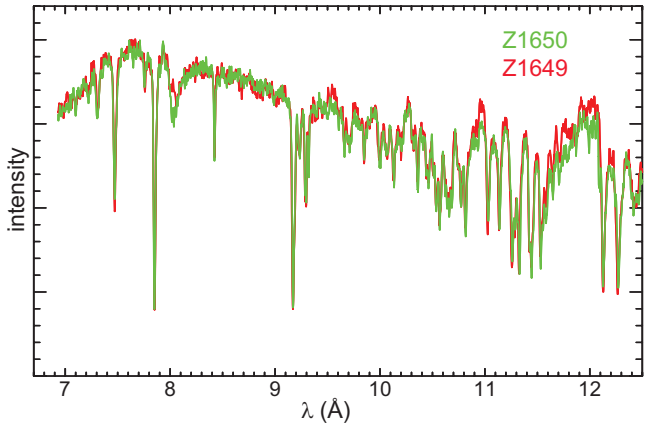

FIG. 7. (Color) Comparison of absorption spectra from two sequential Z experiments. No scaling or other intensity adjustments were applied in this comparison, other than correcting both spectra for the film response.

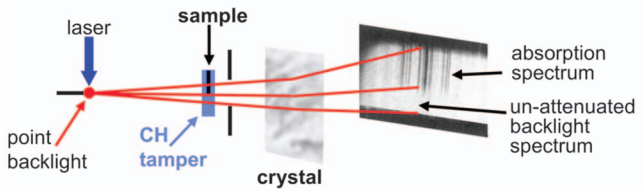

FIG. 8. (Color) Diagram of the experiment configuration used in point projection opacity measurements (adapted from Ref. 22).

backlighting[21,22] provides the required data in a single experiment (Fig. 8). This technique offers the potential for high accuracy without the need for reproducibility, at the cost of increased complexity.

The three main requirements for opacity experiments are as follows:

(1) uniform sample plasma,
(2) accurate transmission measurements,
(3) independent plasma diagnostics,

as succinctly described in Ref. 23. Most research to date has compared the data with models that assume the LTE approximation is valid. In this approximation the ion energy level populations are described by a Boltzmann distribution. Methods for evaluating the validity of this approximation are described elsewhere.[24,25]

Techniques for opacity research were developed using laser-driven experiments beginning in the mid-1980s.[26] The earliest work used a single-sided x-ray source to heat samples composed of Al, Fe, Br, or Ge.[26–30] Later, x-ray cavities known as *Hohlraums* were used to provide a nearly isotropic heating x-ray flux and the variety of sample materials was expanded.[31–36] Crystal spectrometers recorded photons between 1200 and 3000 eV, the electron temperature was 20–76 eV, and the electron density was roughly $(2-4)\times10^{21}$ cm^{-3}. This work established most of the principles used today for opacity research and valuable initial opacity model tests were conducted. However, the crystal spectrometer measurements were unable to address the 40–600 eV photon energy range that dominates the transport at these relatively low temperatures. In later work,[37–39] similar x-ray techniques were used to heat Fe samples, but the spectra were recorded using variable-line-spacing grating spectrometers. This enabled recording 80–300 eV photon energies that are near the peak of the Rosseland mean weighting function. These methods were adapted[40] to the larger x-ray flux provided by the Saturn Z-pinch facility, where a lower density LTE plasma near the conditions that exist in the envelopes of pulsating Cepheid variable stars was studied. These measurements provided strong evidence for the validity of the Opal opacity model[41] in this low temperature low density regime. The Opal opacities helped resolve[42] long standing discrepancies between stellar evolution and pulsation models.

In order to test opacity models used in stellar interior, inertial fusion, and Z-pinch research, higher temperature plasmas are required. Recent experiments[19,20] have exploited the intense radiation created by a dynamic *Hohlraum* x-ray source[43–47] driven by the 21×10^6 Ampere current provided

by the Z facility.[48] This source is formed by accelerating an annular tungsten plasma onto a low density CH_2 cylindrical foam located on the axis. The impact of the tungsten on the foam generates shock radiation that is trapped by the tungsten plasma. This is called a "dynamic" *Hohlraum* because the diameter shrinks with time as the tungsten continues to be compressed by the magnetic pressure supplied by the large axially directed current. An opacity sample placed above the *Hohlraum* end cap is heated by the *Hohlraum* x rays and it is backlit when the radiating shock stagnates on the cylinder axis. These experiments measured Fe transmission at $T_e = 156 \pm 6$ eV, temperatures high enough to produce the charge states, and electron configurations that exist at the base of the solar convection zone (Fig. 5). As mentioned above, the density in these experiments is roughly an order of magnitude lower than at the CZ boundary.

IV. OPACITY EXPERIMENT REQUIREMENTS: SAMPLE UNIFORMITY

A more general expression for the transmission is

$$T(\nu) = \exp\left\{-\int \kappa[\nu, T_e(x), n_e(x)]\rho(x)dx\right\}, \quad (3)$$

reducing to Eq. (1) only if the effect of plasma nonuniformities is negligible. If nonuniformities exist it may still be possible to acquire valuable opacity information by numerically evaluating the integral in Eq. (3). An example of this approach is described in Ref. 35. There, the goal was to produce high densities and gradients were an acceptable tradeoff. Such tradeoffs are sometimes necessary as incremental progress is made toward more extreme conditions. However, the desired accuracy for validating opacity models is high and experiments with significant nonuniformities are unlikely to provide definitive conclusions about the underlying physics embedded within the model.

Volumetric heating by x rays is used to produce uniform hot opacity samples.[49] This is accomplished when a portion of the heating x-ray spectrum streams through the sample. In this case the sample is said to be "optically thin" to at least a portion of the heating x-ray spectrum. This is illustrated for the Z-pinch dynamic *Hohlraum* iron opacity experiments in Fig. 9. A Planckian heating spectrum at radiation brightness temperature $T_r = 200$ eV peaks at $h\nu_{\max} \sim 2.8^* T_r \sim 550$ eV. The optical depth of the initially room temperature sample is less than one, and consequently the transmission is high, over a broad photon energy band near the peak of the heating spectrum. As the sample temperature increases, the opacity drops further and the sample becomes even more transparent near the peak of the heating x-ray spectrum. Thus, photons deposit energy throughout the sample during the entire history of the experiment. This produces uniform heating, at the cost of an inefficient process. The desire for uniform samples is a major reason why large HED facilities are required for high temperature opacity experiments. Note that if the heating spectrum peaks at lower photon energy, then the initial energy deposition may occur primarily near the surface and the sample heating may initially be nonuniform. In this case a detailed consideration of the radiation hydrodynamics of the sample evolution may be needed.

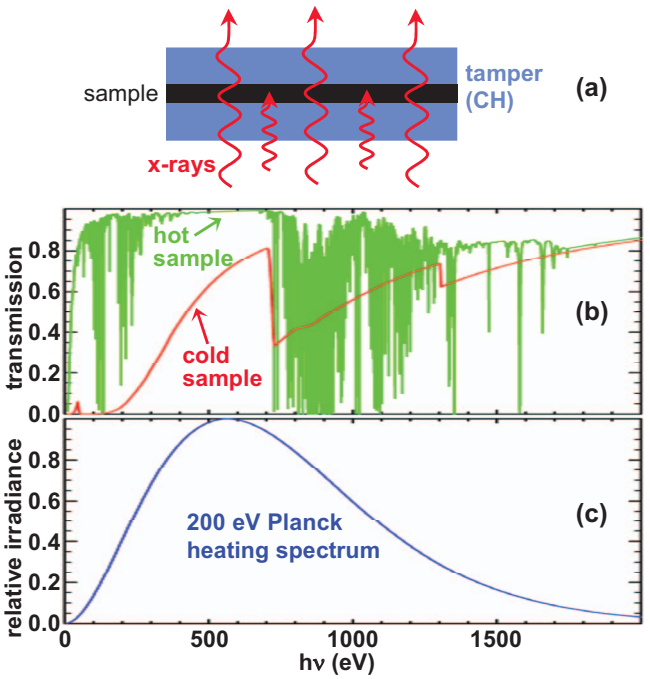

FIG. 9. (Color) X-ray heating provides the ability to volumetrically heat opacity samples (a). A significant portion of the heating x rays stream through the sample, providing relatively uniform but inefficient heating. Transmissions through room temperature iron/magnesium foil and iron/magnesium plasma heated to 150 eV are shown in (b), compared to the heating x-ray spectrum provided by a 200 eV Planckian source (c). The areal density and composition of both the room temperature foil and the plasma are the same as in Refs. 19 and 20.

Temporal uniformity is just as important as spatial sample uniformity. Hot samples inevitably evolve with time and opacity measurements must employ some form of time resolution. The most common technique is to use a short duration backlight source. This allows using film-based detectors, which offer the best spectral range and resolution for typical spectrometer dispersions. Time-resolved detectors are another option. In either case, the temporal evolution of the sample temperature and density must be slow enough that the transmission variation is small over the time scale of the measurement. This favors longer duration, slowly changing x-ray heat sources.

Radiation hydrodynamics simulations have been used to evaluate sample uniformity. While such simulations provide valuable insight, the fact that they necessarily employ the opacity models that are the subject of the test compounds concerns over whether the simulations provide an accurate representation of reality. Given its importance, it is desirable to measure the uniformity. Unfortunately, to date direct uniformity information obtained in opacity experiments has been limited. Perhaps the best certification available has been the determination that spectra used to diagnose the plasma (Sec. VII) are quantitatively consistent with single values of the temperature and density. Future experiments may be able to determine the uniformity directly, for example with space-resolved measurements such as radiography or x-ray Thomson scattering. A significant challenge in this regard is the

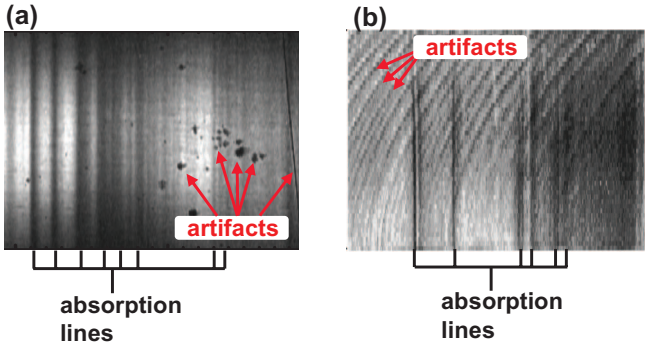

FIG. 10. (Color) X-ray absorption spectra exhibiting reflectivity defects that may masquerade as spectral lines. The image in (a) is from Z experiments (Refs. 19 and 20) and the image in (b) is adapted from Ref. 23. Vigilance is required in experiments to ensure that such defects do not introduce artifacts into the inferred transmission.

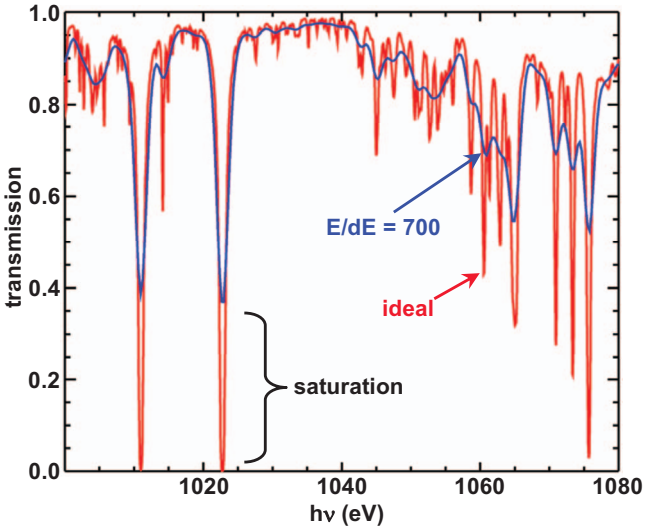

FIG. 11. (Color) Calculated (Ref. 18) transmission for iron plasma at the experimental conditions in Refs. 19 and 20. The blue curve is the ideal case and the red curve accounts for an instrument spectral resolution $E/dE = 700$.

need for spatial resolution of a few microns. A possible solution may be spectroscopy of different tracer elements buried within the sample at specific depths. A problem with this approach is that each tracer absorbs a portion of the heating x-ray spectrum and consequently tracers buried near the rear of the sample are not necessarily heated to the same extent as tracers near the front.[50]

V. OPACITY EXPERIMENT REQUIREMENTS: ACCURATE TRANSMISSION MEASUREMENTS

Numerous technological challenges must be overcome to produce accurate transmission measurements. These challenges may be conveniently divided into concerns arising from the backlight, the sample fabrication, and the spectrometer. Here we restrict the discussion to backlight and spectrometer issues and we consider only crystal-based instruments operating in the 700–10,000 eV photon energy range. Many crystal types and geometrical configurations have been employed in these spectrometers. A problem common to all of them is spectral artifacts arising from crystal defects. Examples of such artifacts are illustrated in Fig. 10. These defects can masquerade as spectral features and care must be exercised to ensure that the inferred transmission is not contaminated by them. The defects are usually obvious in the two-dimensional spectral images (Fig. 10), even though they may not be so easy to identify in a lineout. One possible approach is to examine the spectrum in detail, identify the artifact features, and edit or smooth the spectrum to remove their effect. An alternative is to perform multiple reproducible experiments using different crystals or different crystal alignments, so that the features change from one measurement to another. Then averaging the measurements together effectively removes their influence. The best method to avoid this problem is to procure and characterize the best possible crystals, but perfection in this regard is elusive.

A second spectrometer-related issue that influences accuracy is the finite spectral resolution. Transmission spectra that illustrate the influence of spectral resolution are shown in Fig. 11. The red curve is iron plasma transmission calculated for the Z facility experiment[19,20] conditions using the PrismSPECT model[18] without considering instrument resolution. The blue curve includes a typical resolution of $E/dE \sim 700$. Spectral lines with optical depth greater than one are optically thick and the transmission at line center approaches zero. However, if the line profile is not experimentally resolved, then the observed transmission will be significantly larger. Such lines are said to be "saturated."[51] Saturation effects must be incorporated into comparisons with opacity models. These effects are one reason opacity model calculations are converted into transmission for comparison with data, rather than the measured transmission being converted into opacity. Once the instrument blurring occurs, information is lost and it cannot be recovered. Deconvolution may be feasible, but it typically introduces unacceptable uncertainties. If it is desired to compare opacities rather than transmission, the opacity calculations must first be converted to transmission, the instrument resolution convolved, and then reconverted back into opacity. Thus, it is simpler and generally more informative to compare transmissions. Ultimately, the two key points of this discussion are that instrument resolution must be measured and higher spectral resolution is desirable. However, resource limitations often restrict spectral resolution measurements to relatively few photon energies, despite the fact that spectral resolution is a function of photon energy. If the measured spectral range is relatively small, then the impact of spectral resolution uncertainty may be negligible. In other cases the portion of the transmission uncertainty that arises from the spectral resolution uncertainty may be significant.

A third technological challenge associated with the spectrometer is the type of detector used. Time-resolved detectors such as streak cameras or microchannel plate (MCP) cameras have been successfully used in some experiments.[37,40,52] These detectors may be essential for rapidly evolving sample conditions or if the late-time sample self-emission is bright enough to compete with the backlight (see discussion of self-emission effects below). However, the active area of such

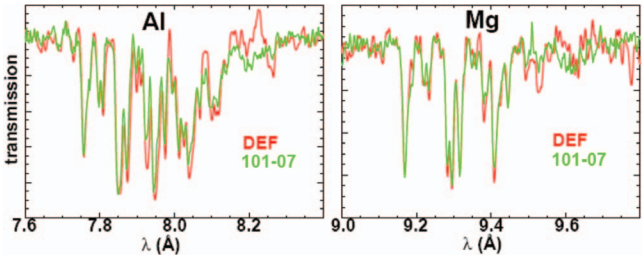

FIG. 12. (Color) Comparison of x-ray absorption spectra recorded on two different types of film, Kodak DEF and 101–07. The agreement between the two implies that the conversion of film density to film exposure was self-consistent.

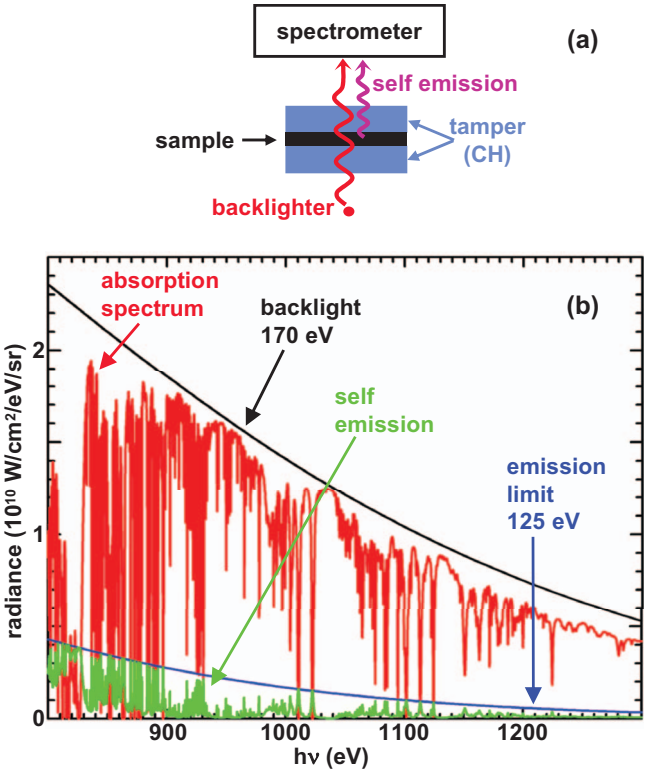

FIG. 13. (Color) Self-emission can contribute to the signal recorded by the spectrometer (a). A hypothetical situation is quantitatively illustrated in (b) using PrismSPECT (Ref. 18) calculations for iron plasma self-emission (green curve) and absorption spectra (red curve). The plasma temperature is assumed to be 125 eV and the backlighter is assumed to be a 170 eV Planckian. The most optically thick lines have self-emission that peaks at the blackbody limit, corresponding in this case to a 125 eV Planckian.

detectors often restricts the spectral range. An effort to circumvent this problem with large format MCP configurations is underway.[52,53] Nevertheless, the spatial resolution element size of existing time-resolved detectors is approximately 80 μm or larger. This limits the spectral resolution that can be achieved in most cases. The detector used in most opacity experiments to date has been x-ray film. Film has the advantage of larger effective number of pixels. Spatial resolutions of 5 μm are routinely available. However, film has the disadvantage of nonlinear response and it requires both accurate calibrations and careful attention to developing procedures. Calibrations are resource intensive and rarely performed. This raises a concern that the film sensitivity may change, especially since film manufacturers regard film design and fabrication details as proprietary. For example, the most commonly used x-ray film calibrations are those of Henke *et al.*,[54,55] performed more than twenty years ago. In order to evaluate concerns over possible film development or fabrication problems, an experiment using two different types of x-ray film was performed using a tamped Al and Mg opacity sample placed to the side of a Z pinch[56] (Fig. 12). The results agree, supporting the sustained validity of the Henke calibrations. Nevertheless, vigilance over film development and possible manufacturing changes is certainly warranted. X-ray charge coupled devices have a linear response and are probably a desirable option to consider in future opacity experiments. Image plates[57] are another attractive detector technology, although not all image plates and scanning systems provide the needed spatial resolution. Sensitivity to high photon energy x-ray backgrounds may also limit the utility of image plates for opacity measurements in the keV photon energy range.

Producing a high quality backlight is a key enabling technology for opacity experiments. The desired characteristics are broad spectral range, a smooth featureless spectrum, and high brightness. Broad spectral coverage is needed both to probe a wide range of features in the element of interest and to measure simultaneously spectral lines in diagnostic tracers added to the sample (see below). A relatively smooth and featureless backlight spectrum is needed because if the backlight spectral features overlap with features in the sample, then the accuracy requirements of measuring the backlighter spectrum increase dramatically. This problem is aggravated by limited instrumental resolution.[58]

High backlight brightness is needed both to supply an adequate exposure at the detector and to overwhelm the sample self-emission.[23] The complications introduced by sample self-emission are illustrated using calculated signals for a hypothetical experiment in Fig. 13. The spectrometer detects the desired backlight photons and also samples self-emission contributions. In Fig. 13(b) example, the backlight source is a 170 eV Planckian and the iron sample temperature is 125 eV. The density and optical path length correspond to typical sample conditions.[19,20] The self-emission and absorption spectra were computed using the PrismSPECT model.[18] The brightest spectral lines emitted by the sample are optically thick and peak at the blackbody limit: a Planckian corresponding to the sample electron temperature.[59,12] The experimental transmission determined from Eq. (1) is affected most for the strongest spectral lines since they have the brightest self-emission. Clearly, the problem is amplified if the self-emission is an appreciable fraction of the backlight. Thus, the problem gets worse as the sample temperature increases (Fig. 14). The self-emission signals from 125 and 150 eV samples are compared to the 170 eV Planckian backlight in Fig. 14(a) and the corresponding transmission with and without the 150 eV sample self-emission is shown in Fig. 14(b). In this case, an inadequate treatment of self-emission would provide misleading information for opacity model comparisons.

The consequences of self-emission are potentially sig-

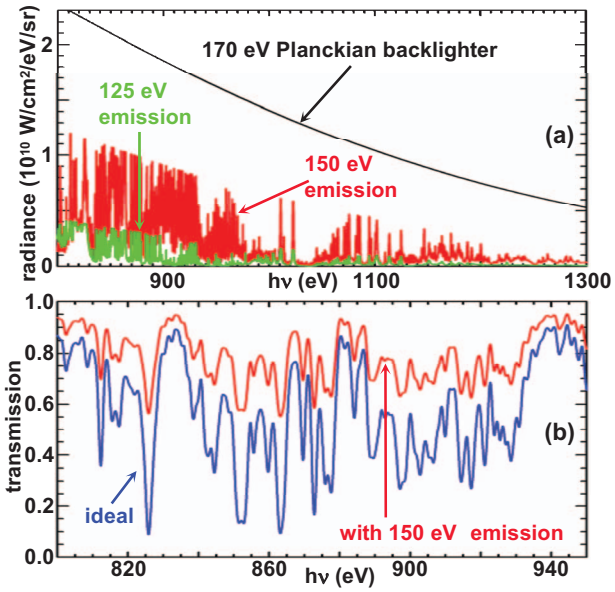

FIG. 14. (Color) Self-emission grows with sample temperature and competes more strongly with a specified backlighter (a). The transmission calculated (Ref. 18) for a portion of the spectrum is illustrated both with and without self-emission in (b). The backlighter was assumed to be a 170 eV Planckian and the sample temperature was 150 eV. Both transmission spectra include convolution with $E/dE=700$ instrument resolution.

nificant and two courses of action are possible to mitigate their effect: the backlight should be rendered much brighter than the sample self-emission and the sample self-emission should be measured during the experiment. Calculations of the self-emission and approximate backlight brightness for the Z facility iron experiment[19,20] are shown in Fig. 15(a). The corresponding transmission with and without the self-emission [Fig. 15(b)] shows that the 315 eV Planckian backlight overwhelms the sample self-emission; thus, it has negligible effect on the transmission. The sample self-emission and absorption can be measured using the same spectrometer as long as the spatial extent of the backlight is small compared to the size of the heated sample. Both the space-resolved spectrometer and point projection configuration enable the self-emission to be recorded. These self-emission measurements require high detector dynamic range since we desire self-emission that is less than a few percent of the backlight.

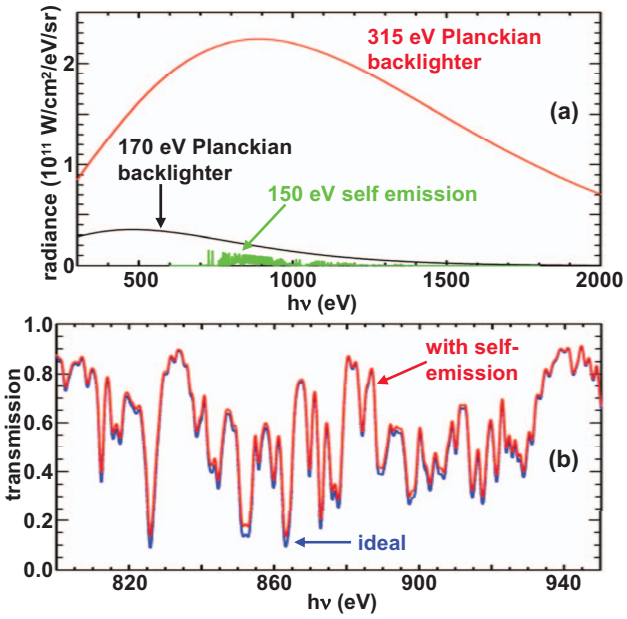

FIG. 15. (Color) Self-emission from iron plasma at 150 eV electron temperature is compared with 170 and 314 eV Planckian backlighter spectra in (a). The ideal transmission without self-emission and the transmission including self-emission are almost the same if the backlighter spectrum corresponds to a 314 eV Planckian (b). Both transmission spectra include convolution with $E/dE=700$ instrument resolution.

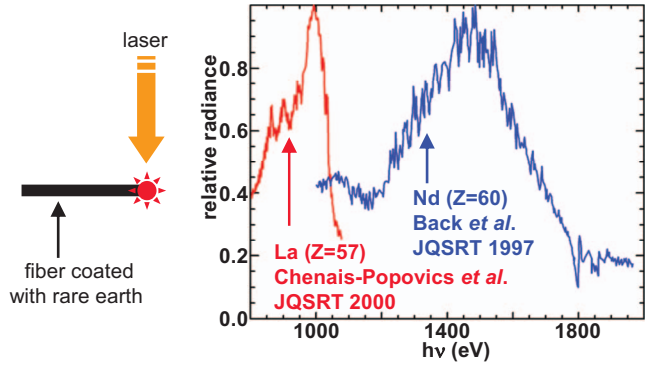

FIG. 16. (Color) Pioneering opacity experiments primarily used laser heated fibers coated with rare-earth elements to produce the backlighter. The La spectrum is adapted from Ref. 31 and the Nd spectrum is adapted from Ref. 34.

The quest for a high brightness, broad spectral coverage, and a spectrally featureless backlight is an ongoing topic in opacity research. Early efforts produced pointlike bright sources by irradiating small fibers with lasers. Emission in the desired spectral range was obtained by coating the fiber with a high Z material[26,31,34] often a rare-earth element (Fig. 16). The emission from these high Z laser produced plasmas consists of many millions of spectral lines that blend into unresolved transition arrays (UTAs). The $3d$-$4f$ UTAs are particularly bright and can backlight an approximately ~200–400 eV range in the 1–3 keV photon energy regime. In addition, these sources are inherently spectral line sources and very careful measurements are required to account correctly for the spectral structure. This introduces a potential systematic error that is hard to quantify.

Recent opacity research has emphasized the development of backlight sources that span a larger photon energy range and that are inherently continuum emission sources. This is challenging because bright sources are required. As laser facilities grow in energy it may be possible to create "conventional" *Hohlraums* that reach high brightness temperatures.[60] The most successful approach to date has been the production of dynamic *Hohlraums* driven either by high power Z pinches or lasers. These sources are heated by a radiating shock. The shock emission is trapped by a high Z plasma that is compressed over time. The use of a Z pinch to create such a source was briefly described above and more details are given in Ref. 20. Spherically convergent dynamic *Hohlraums* have also been produced at the Omega laser facility.[61] In these experiments the laser typically illuminates a spherical plastic shell filled with xenon gas. The emission

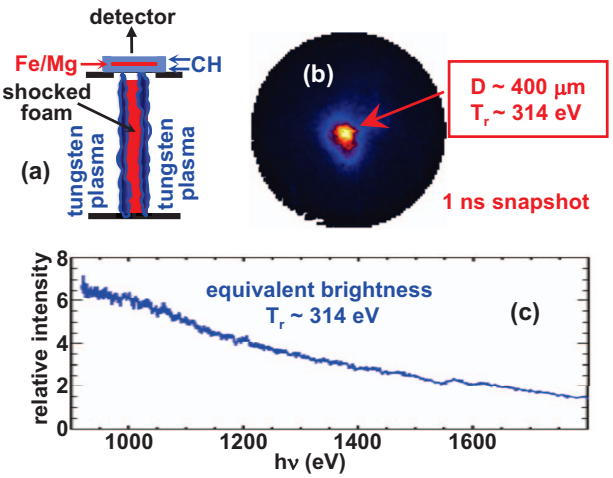

FIG. 17. (Color) Dynamic *Hohlraum* backlighter diagram (a). The stagnation of a radiating shock on the pinch axis produces a bright continuum source. A time-gated x-ray pinhole image is shown in (b) and a plot of relative intensity as a function of photon energy is shown in (c).The equivalent brightness temperature is $T_r \sim 314$ eV (Ref. 20).

from the shock launched into the xenon is trapped because of the high opacity of the xenon plasma behind the shock.

The Z-pinch driven dynamic *Hohlraum* described above used the Z facility to produce a backlight with peak radiation temperature of approximately 314 eV.[20] This backlight spans an effective range of $h\nu \sim 800-2000$ eV, it is essentially line-free, and it is bright enough to backlight samples at temperatures up to ~ 160 eV (Fig. 17). The characteristics of the Omega laser-driven backlight in the 800–2000 eV spectral range that is of interest for opacity experiments at $T_e = 100-160$ eV have not been published. However, measurements at higher photon energies have been documented[61] and the characteristics of this source for future experiments may be attractive.

VI. OPACITY EXPERIMENT ACCURACY EVALUATION

Performing high accuracy opacity experiments is not simple since many potential pitfalls exist. However, a relatively straightforward method[23] is available to experimentally assess the accuracy of the measurements. The method depends on Beer's law relationship [Eq. (1)] between transmission and sample thickness. Suppose we measure transmission through two uniform samples with identical conditions but with different thicknesses x_1 and x_2. The transmission through sample 2 is related to the sample 1 transmission by $T_2 = T_1^{(x2/x1)}$ (Fig. 18). Measuring the transmission through different thickness samples and evaluating whether the scaling obeys Beer's law is an extremely effective means to assess possible errors. Problems that will cause deviation from Beer's law include sample nonuniformity, self-emission, background subtraction, crystal artifacts, and inaccurate film response corrections. For example, if the heating x rays deposit more energy near the front sample edge and produce nonuniform conditions, then the nonuniformity will be worse with increasing sample thickness and the transmission will deviate from the expected scaling. As another example, the sensitivity of the transmission to self-

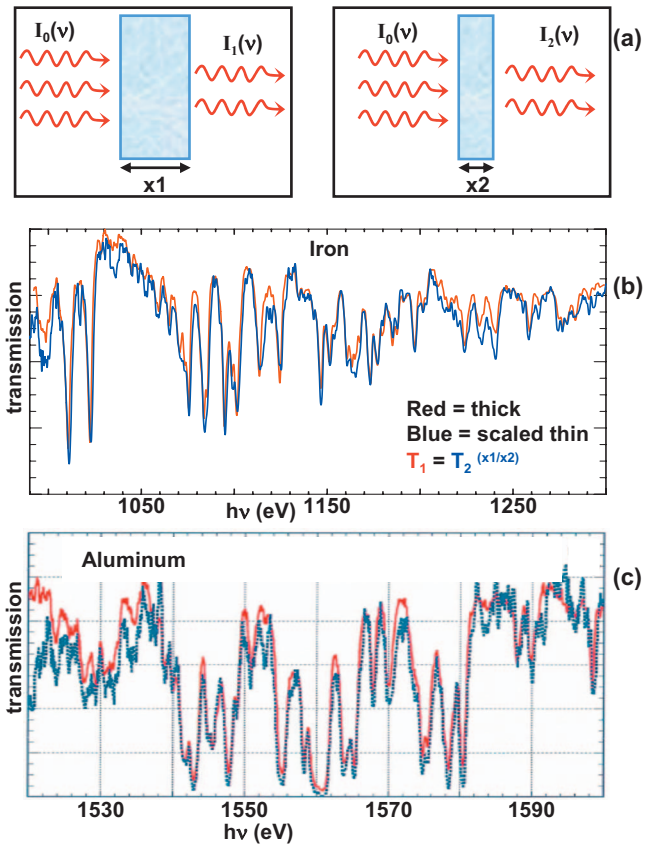

FIG. 18. (Color) Evaluation of transmission accuracy using experiments with different thickness samples (a). Examples of experiments that demonstrated high quality using the sample thickness scaling method are shown in (b) and (c), adapted from Refs. 19 and 62, respectively.

emission problems depends on the optical depth and thus the sample thickness. As a third example, artifacts that are introduced because of crystal defects will not change when the sample thickness changes and examination of transmission scaling with thickness therefore serves to identify those artifacts. Finally, the exposure at the detector will depend on the sample thickness and verification that transmission scales correctly according to Beer's law can detect inaccuracies in the conversion of film density to exposure. A host of problems can be detected with such scaling tests and the tests are straightforward to perform. One limitation is that problems arising from insufficient spectral resolution when narrow spectral features in the backlight and sample coincide are not detectable.[58] Furthermore, performing scaling tests requires greater resources, since either additional experiments or more complicated targets are needed. Two experiments[19,62] which demonstrated a high degree of scaling accuracy are shown in Figs. 18(b) and 18(c). Note that in these experiments both the weak and strong absorption features exhibit accurate scaling. This is significant because many of the problems that might arise preferentially affect either the strong or weak features, altering the *relative* absorption strengths.

The transmission scaling described above is the most powerful test to evaluate experiment accuracy. Supplemental valuable information may also be obtained by performing multiple measurements within each experiment and/or mul-

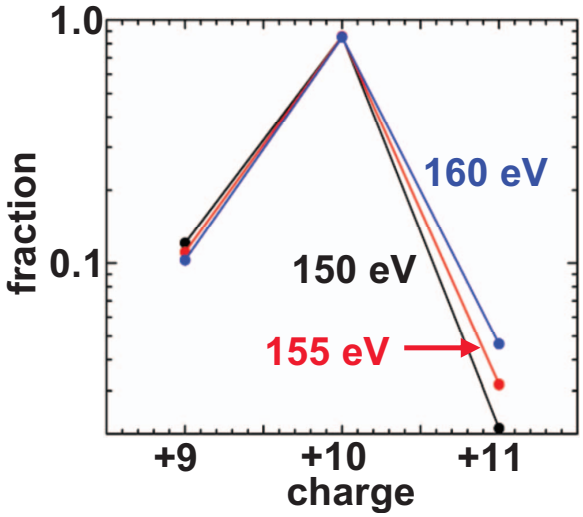

FIG. 19. (Color) Calculated (Ref. 18) charge state distribution for Mg at 150 eV (black), 155 eV (red), and 160 eV (blue) electron temperatures. The electron density was 7×10^{21} cm^{-3} in all cases. These ±5 eV temperature changes induce less than 1% change in the He-like Mg(Mg^{+10}) population, but the H-like Mg(Mg^{+11}) population changes by approximately ±40%. The Li-like Mg(Mg^{+9}) population changes by a smaller amount.

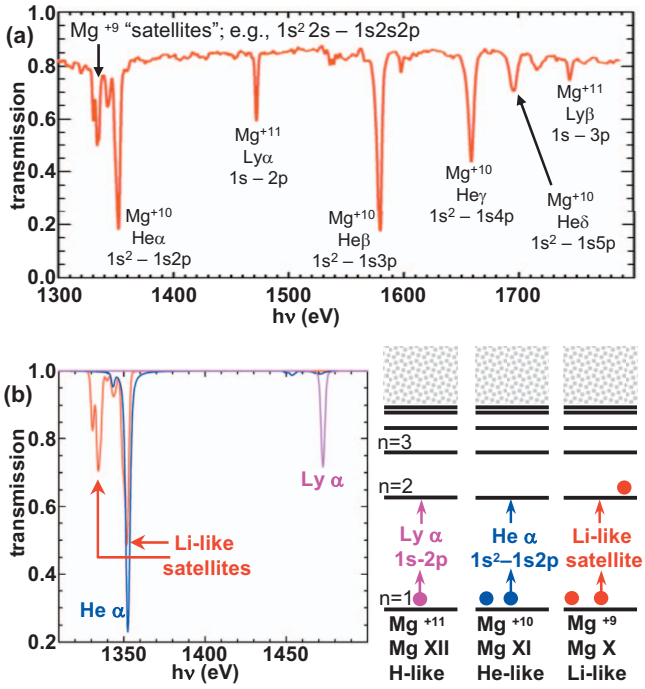

FIG. 20. (Color) Typical K-shell absorption spectrum with features from H-, He-, and Li-like Mg (a). The spectrum in (a) represents the average transmission from the experiments in Ref. 19. PrismSPECT calculations of an expanded view of the $n=1$ to $n=2$ transitions in these three charge states and a simplified energy level diagram illustrate the energy shift from nuclear screening by additional spectator electrons in He-like and Li-like ions (b).

tiple reproducible experiments. Multiple measurements using varying detector sensitivity provides signals recorded at different exposure levels. Comparison of the measurements therefore reveals whether detector response is linear or if film density-to-exposure conversions have been accurately performed. Multiple measurements using different crystals can reveal whether crystal artifacts have affected the results. Averaging the results of multiple reproducible experiments improves signal-to-noise values[19] and can be essential for accurate transmission measurements of weak spectral features.

VII. PLASMA DIAGNOSTICS

Opacity is a function of the plasma electron temperature and density and quantitative opacity model tests require sample characterization. Here, we emphasize electron density rather than mass density since it is the electron density that directly affects the collisional ionization and excitation rates. Plasma diagnosis often relies on K-shell absorption spectra under the assumption that the models used to interpret these relatively simple spectra are reliable. The details of K-shell spectral diagnostics are described elsewhere[63–66] and we provide only a brief review of the physical basis for K-shell spectral diagnostics.

The value of K-shell spectra to diagnose electron temperature depends on two facts. First, the plasma ionization distribution is a strong function of the electron temperature but has a weak dependence on the electron density (Fig. 19; see also Fig. 5). Second, the K-shell spectral line photon energies shift with ionization. The former means that the relative absorption strengths of K-shell spectral lines from different charge states depends on electron temperature. The latter means that the features from particular charge states are readily discerned from each other. K-shell spectral absorption lines are defined as lines with an initial principal quantum number $n=1$. Absorption transitions between the $1s$ and $2p$ configurations are possible if there are vacancies in the $n=2$ shell. Thus, K-shell absorption may arise in atoms ionized into either the K- or L-shell. These transitions are conveniently divided into two classes according to whether they occur in K-shell (H- and He-like) ions that have only one or two bound electrons or L-shell (Li-, Be-, B-, C-, O-, N-, and F-like) ions that have three to nine bound electrons. This distinction has value because the diagnostics available from these two classes are somewhat different. Both these transition classes can diagnose T_e, with comparable accuracy. In addition, transitions between the $1s$ or $1s^2$ ground states and the $n=2$ or 3 levels are affected by Stark broadening[67] and provide valuable density information, as described below. However, the Stark broadening of L-shell ions has not been used extensively and its reliability is less certain.

A measured K-shell transmission spectrum formed by the H-, He-, and Li-like charge states of Mg is shown in Fig. 20(a). The bound-bound transitions that contribute $n=1$ to $n=2$ spectral lines are displayed with a calculated synthetic spectrum in Fig. 20(b). The strongest absorption line from H-like ions is the $1s$-$2p$ transition, known as Lyα, while the strongest line from He-like ions is the $1s^2-1s2p$ transition, known as Heα. The Heα photon energy is ~120 eV lower than the Lyα because of the nuclear screening provided by the second $1s$ electron. Similarly, the $1s^22s-1s2s2p$ Li-like transition has lower photon energy than Heα, but the energy separation between the Li-like lines and Heα is only of order 15–20 eV because the additional screening by the $2s$ electron is less than that by the $1s$ electron. The extra electron that

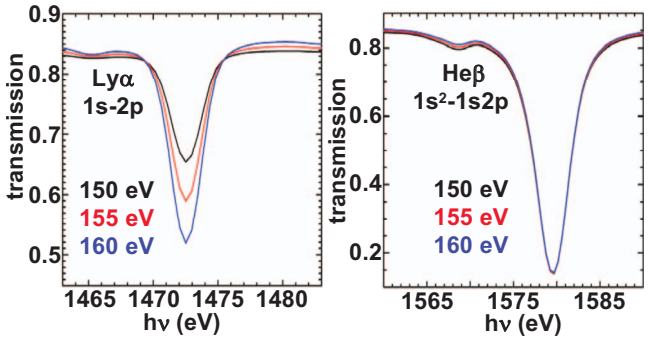

FIG. 21. (Color) Calculated (Ref. 18) absorption from Mg Lyα and Heβ at the three temperatures corresponding to Fig. 19 charge state distributions. The $E/dE=700$ instrument resolution effect is included.

does not participate in the transition is sometimes referred to as a "spectator" electron and these Li-like lines are known as "satellites" because they appear near the resonant Heα transition. The Li-like spectator electron may also reside in an excited $n=3$ (or higher) state. In this case the satellite transitions are only slightly shifted from the Heα photon energy and these lines may not be resolved [Fig. 20(b)]. A careful accounting of this transition blending must be incorporated into accurate plasma diagnostics. Note that He-like satellites also appear on the low photon energy side of Lyα, arising from initially excited He-like configurations (e.g., $1s2s-2s2p$). Satellite lines often provide additional valuable diagnostics because they depend on the mechanism that populates the excited states.

The sensitivity of typical H- and He-like Mg ion spectral lines to small temperature changes is illustrated in Fig. 21. This example is drawn from the Z experiments[19,20] investigating iron opacity models and we employ the Heβ ($1s^2-1s3p$) transition because iron spectral lines are blended with the Heα. The Heβ absorption line strength is not sensitive to changes in temperature because the fractional population of the closed-shell He-like Mg ions changes very little

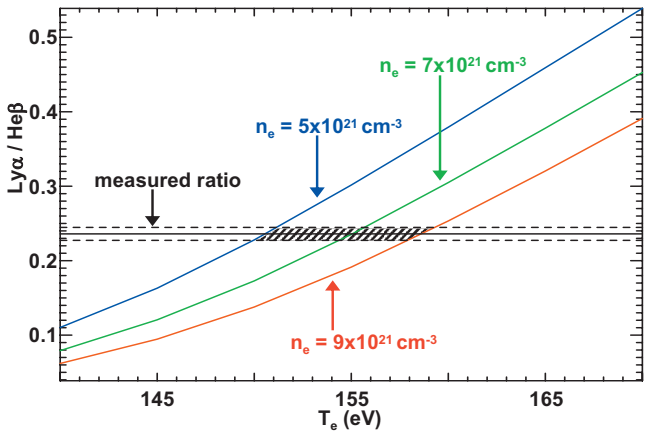

FIG. 22. (Color) Calculated Mg Lyα/Heβ absorption line strength ratio as a function of electron temperature. The three curves correspond to three different electron densities. The horizontal line corresponds to the mean ratio value measured in the experiments in Refs. 19 and 20 and the dashed lines are the $\pm 1\sigma$ ratio uncertainties. The experimental temperature lies within the cross-hatched region.

in this temperature range. On the other hand, the Lyα absorption changes rapidly with temperature. Thus, measurements of the integrated Lyα/Heβ absorption line strength ratio provide a temperature diagnostic (Fig. 22). The three different curves in Fig. 22 correspond to three different electron density values, illustrating the simultaneous dependence of the ionization distribution on both temperature and density mentioned above. In this case a $\pm 30\%$ change in electron density alters the inferred temperature by approximately ± 3–4 eV. Thus, accurate temperature diagnostics using this method depend on knowledge of the electron density.

Preliminary temperature estimates may be obtained by a visual comparison of measured and synthetic spectra calculated at different temperatures. However, quantitative opacity model tests require estimates for the temperature and density uncertainties. These may be obtained using the spectral line fitting techniques described in Refs. 20 and 68 to determine the uncertainties in the measured absorption line strengths. High quality measurements combined with careful analysis may provide temperature values accurate to typically $\pm 5\%$, with roughly half the uncertainty arising from the typical $\pm 30\%$ density uncertainty and the other half from the absorption line measurement accuracy. Note that these estimates do not include any uncertainty associated with the spectral synthesis model used to interpret the data. The systematic model errors can be reduced by using as many line ratios as possible to infer the temperature, reducing the probability that transition rate errors for any single line might bias the results. Analysis performed with several different K-shell opacity models can also solidify the reliability of the temperature result, although the extra resource investment renders this type of duplicate analysis uncommon.

The class of transitions in ions with three to nine bound electrons is still reasonably simple and the ionization distribution is typically broader. These ions involve an open $n=2$ shell and they normally possess strong features from four or five charge states. This broader distribution may enhance accuracy and reliability of electron temperature measurements. The transitions involved are generally $1s^2 2s^m 2p^l - 1s2s^m 2p^{l+1}$. These lines are sometimes referred to as "$K\alpha$ satellites" because they appear on the high energy side of the neutral atom $K\alpha$ transition and they were first observed in experiments that directed high energy particle beams onto solid surfaces to investigate $K\alpha$ transitions. As with the transitions described above, the $n=2$ spectator electrons do not participate directly in the transition, but they do provide nuclear screening that shifts the transition energy. This class of transitions is critically important for diagnosing low temperature plasmas (e.g., $T_e < 100$ eV). At low temperatures the simple H- and He-like charge states described above occur only for ions with atomic number less than approximately 10. These low-Z atoms have K-shell lines that appear in the x-ray ultraviolet (XUV) spectral range and are consequently more difficult to measure. $K\alpha$ satellite transitions may be observed in the soft x-ray (>1 keV) range even for temperatures as low as ~ 10 eV.

The diagnostic utility of this type of transition was first developed for emission spectra arising in energetic electron or ion beam experiments[69] and for early laser-driven capsule

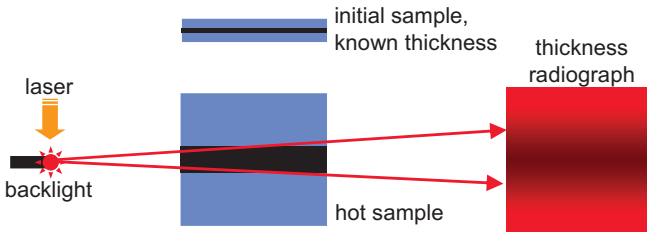

FIG. 23. (Color) Diagram of point projection radiography method used to measure sample expansion and thus measure the sample density. A dispersive element such as a crystal is often inserted in front of the detector to provide spectrally resolved information, greatly enhancing the radiograph contrast.

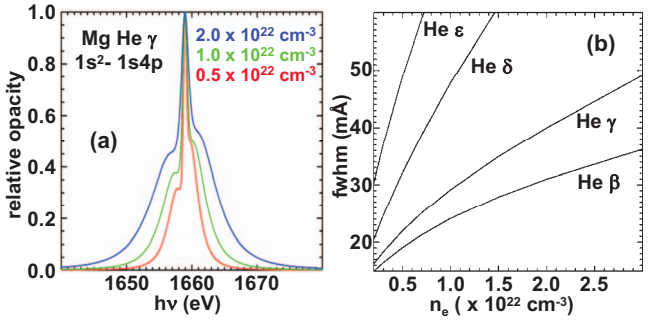

FIG. 24. (Color) Example of Stark-broadened line profile calculations (Refs. 76 and 77) (a). The red, green, and blue curves correspond to 0.5, 1.0, and 2.0×10^{20} cm^{-3} electron densities, respectively. These opacity profiles are converted to transmission and then convolved with the instrument resolution before comparing with the experiment (Ref. 20). The plot in (b) illustrates the full width at half maximum as a function of electron density. The areal density and instrument resolution in (b) correspond to the Z experiments in Refs. 19 and 20.

implosions.[70] Later, it was extensively employed in absorption spectra used to diagnose a wide array of HED experiments, including opacity.[26,71,72] The usefulness of this transition class is also supported by the fact that adjacent $1s$ to $2p$ transitions in Li-like to F-like ions shift enough to be measured, but not so much as to make broad spectral coverage necessary. Thus, such diagnostics are especially appropriate if a more limited spectral range backlight is available. Transitions involving initial states with an excited electron arise in these spectra[73,74] and the resulting lines may blend with lines from the ground state of adjacent charge states. This is similar to the illustration provided above for Li-like ions and this charge state blending must be included in models used to infer temperature from such data. Transitions with higher-n final states (e.g., $3p$) have been observed, but they are typically relatively weak and the models needed to interpret the line broadening are less certain. Consequently, the class of transitions in Li-like to F-like ions has been only rarely employed in plasma electron density diagnostics up until now.[29]

Several types of electron density diagnostics have been developed for opacity experiments. Radiographic measurements of the sample plasma expansion and Stark broadening of K-shell spectral lines are two techniques that provide relatively direct density measurements. Optical laser interferometry measurements of the sample rear surface expansion have also been used to infer opacity sample density.[75] However, the plasma that is actually probed at optical wavelengths is the low density edge of the sample plasma and these techniques must rely heavily on radiation hydrodynamic simulations to infer the behavior of the higher density interior of the opacity sample.

Point projection spectrally-resolved radiography was the first method employed to determine sample density.[21–23] These measurements are conceptually straightforward: The sample thickness is measured after it is heated by the x-ray source and the density is obtained by comparing with measurements of the initial sample thickness performed prior to the experiment (Fig. 23). A major challenge for this method is the experiment complexity introduced by the need to acquire simultaneously an edge-on radiograph and the spectrally-resolved transmission measurement used to infer the temperature and to test the opacity model for the element of interest. Additional problems include accurate initial sample composition and thickness measurements, accuracy limitations imposed by the finite point projection backlight size, assumption of one-dimensional expansion, and simultaneity of the density measurement radiograph with the transmission measurement. Despite these problems, density measurements accurate to approximately $\pm30\%$ have been acquired in a few opacity experiments.

Measurements of Stark-broadened[67] K-shell spectral lines also enable determination of the sample density. Atomic line transitions in tracer ions are perturbed by the electric microfields due to the other electrons and ions in the plasma. The net result is a characteristic Stark-broadened line shape that is mainly dependent on the density. In the standard Stark broadening theory approximation the ions are considered static while the lighter electrons are considered dynamic, i.e., they move while the line transition takes place. The distribution of static ion microfields causes energy levels to split and shift due to the Stark effect of the electric fields. The photon energy of dipole-allowed line transitions shifts accordingly, and the atomic state mixing by the electric field can even cause non-dipole-allowed transitions to appear. In addition, radiator ions experience a time-varying electric field due to the dynamic electrons. This broadens the line transitions that arise between shifted energy levels. The final line shape is obtained by averaging over the distribution function that the weights the static ion microfields according to their probability of occurrence, incorporating the broadening due to the dynamic electrons. Thus, the line profile broadening depends on both the ion and electron density and is typically used to infer the electron density, as long as the plasma composition is known.

Calculations[76,77] of Stark-broadened Mg Heγ line profiles used to diagnose the Z facility iron opacity samples[19,20] are shown in Fig. 24(a). The sensitivity of the line opacity profile to density is clear. However, a complication arises in applying this diagnostic to absorption spectra because the transmission line profile is not the same as the opacity profile.[20,59,78] The transmission $T=\exp\{-\kappa\rho x\}$ is approximately $T\sim1-\kappa\rho x$, if $\kappa\rho x\ll1$. Such a line is said to be optically thin and the transmission profile essentially appears to be an upside down opacity line profile. However, as the optical depth $\tau=\kappa\rho x$ grows to approach and then exceed unity,

this approximation is no longer valid. In this case the transmission profile depends on the optical depth and the areal density ρx of the ions in the lower level of the transition (typically the ground state) is required in order to relate the transmission line profile to the opacity line profile. Fortunately, such knowledge may be reliably obtained by measuring the integrated strength of the absorption line family that arises from a given charge state. Once the optical depth has been determined, the transmission may be computed from the opacity profile. Convolution with the instrument function must be performed prior to comparison with measured spectral line profiles. The dependence of He-like Mg spectral linewidths on electron density is illustrated for the Heβ, Heγ, Heδ, and Heε lines in Fig. 24(b). The widths in Fig. 24(b) correspond to transmission widths after convolution with the instrument function. They include the optical depth effect and instrument widths appropriate for the Z iron opacity experiment.[19,20] A more detailed description of this procedure is given in Ref. 20.

Stark broadening increases and the opacity decreases with principal quantum number. Thus, both the ability to resolve the profile and the problems introduced by the requirement for areal density information to interpret optically thick line broadening favor the use of high n spectral lines. However, high-n spectral lines are typically weaker and therefore they are measured less accurately. The most accurate density diagnostics are obtained by measuring as many lines as possible and quantitatively accounting for the signal-to-noise ratio.[20] Typical density accuracy obtained with this method is $\pm 30\%$. However, this does not account for possible uncertainties introduced by the Stark broadening models. Stark broadening measurements of HED plasma densities have been performed for more than 2 decades and calculations of H-like and He-like profiles are generally considered reliable. However, only limited experimental information directly designed to test broadening models in this density regime is available[79] and future opacity research would benefit from more extensive tests.

VIII. STATUS AND FUTURE PROSPECTS FOR HED PLASMA OPACITY RESEARCH

The methods described above provide a framework for experiments designed to test opacity models. However, the range of temperatures, densities, and elements examined up until now is small. The vast majority of experiments investigated plasmas with 20–76 eV temperatures and $0.01-0.03$ g/cm^3 mass densities. Only a few experimental results exist outside of this range. Examples include the Saturn Z-pinch driven experiments[40,42] that investigated iron opacities for envelopes of Cepheid variable stars and the Z facility experiments investigating opacity of the iron charge states that exist at the base of the solar convection zone.[19,20] The former extended the density range down by two orders of magnitude while the latter pushed the temperature range up by approximately a factor of 2. These experiments provided valuable opacity model tests, yet they are probably best regarded as proof-of-principle experiments that establish platforms for further investigations. Comprehensive results require more experiments.

The parameter space of applications that would benefit from opacity experiments is large. Here, we mention only a few obvious examples that might be addressed within the coming years. We also reiterate that, while applications provide important motivation that guides research directions, advances in opacity science require sustained focus on the physics within the opacity models. The discrepancies between helioseismology and solar models motivates investigations of iron plasma opacity at temperatures similar to the existing Z facility experiments, but at densities an order of magnitude higher. Measurements of oxygen and neon opacities are also needed, even though the atomic physics of the K-shell is more certain than the Fe L-shell. For example, the bound-free opacities of these elements play an important role in the total opacity. The bound-free process is important over a large photon energy range, implying that a relatively small error might have important consequences. Furthermore, atomic physics is just one issue. Questions also remain regarding the accuracy of ionization distribution calculations.[80] Finally, opacity experiments to date have measured either pure elements or mixtures of two similar atomic number elements. It is a fair question to ask whether the model treatments mid-Z elements mixed as dilute constituents in a mostly hydrogen plasma are adequate.

Inertial fusion capsule implosion designs typically employ Be shells doped with Cu or CH shells doped with Ge. The motivation for the dopants is to modify the ablation pressure as a function of depth using the opacity changes caused by introducing the dopant. Thus, the success of these capsule designs depends on accurate knowledge of the dopant opacity in the 50–300 eV temperature range, at a variety of densities between 0.01 and 10.0 times solid. Experiments have measured Ge opacity at temperatures up to 76 eV and densities of approximately 0.01 solid. These investigations provided initial tests of basic opacity model questions. However, these experiments did not measure the charge states and electron configurations that will arise in inertial fusion implosions. Furthermore, to the best of our knowledge, Cu transitions have not been measured at all, let alone Cu diluted in a mostly Be plasma at high temperature and density. Improved opacity knowledge would enable experimenters to emphasize other issues such as laser plasma interaction or equation of state in tuning inertial fusion implosions to reach ignition. The opacity research methods developed over the past 20 years, combined with the advent of megajoule class HED facilities, should enable near-term opacity investigations for matter found in stellar interiors, inertial fusion implosions, and Z pinches.

ACKNOWLEDGMENTS

We thank the Z facility teams for invaluable and dedicated technical assistance. Special assistance was provided by P. W. Lake, D. S. Nielsen, L. Nielsen-Weber, and L. P. Mix. We are grateful to R. J. Leeper, T. A. Mehlhorn, J. L. Porter, and M. K. Matzen for support and encouragement. Special thanks are due to T. S. Perry, C. Back, and F. Gille-

ron for gracious permission to share previously published results here. Sandia is a multiprogram laboratory operated by Sandia Corporation, a Lockheed Martin Co., for the United States Department of Energy under Contract No. DE-AC04-94AL85000. Work by CAI performed under the auspices of the Department of Energy by Lawrence Livermore National Laboratory under Contract No. W-7405-ENGF-48.

[1] A. S. Eddington, *The Internal Constitution of the Stars* (Cambridge University Press, Cambridge, 1926).
[2] F. Delahaye and M. Pinsonneault, Astrophys. J. **625**, 563 (2005).
[3] D. Mihalas, *Stellar Atmospheres* (W.H. Freeman, San Fransisco, 1970).
[4] J. N. Bahcall, A. M. Serenelli, and S. Basu, Astrophys. J. **621**, L85 (2005); J. N. Bahcall, W. F. Huebner, S. H. Lubow, P. D. Parker, and R. K. Ulrich, Rev. Mod. Phys. **54**, 767 (1982); see: www.sns.ias.edu/~jnb.
[5] S. Basu and H. M. Antia, Phys. Rep. **457**, 217 (2008).
[6] M. Asplund, Annu. Rev. Astron. Astrophys. **43**, 481 (2005) (and references therein).
[7] J. N. Bahcall, A. M. Serenelli, and M. Pinsonneault, Astrophys. J. **614**, 464 (2004).
[8] S. Turck-Chieze, S. Couvidat, L. Piau, J. Ferguson, P. Lambert, J. Ballot, R. A. Garcıa, and P. Nghiem, Phys. Rev. Lett. **93**, 211102 (2004).
[9] H. M. Antia and S. Basu, Astrophys. J. **620**, L129 (2005).
[10] S. Basu and H. M. Antia, Astrophys. J. **606**, L85 (2004); J. N. Bahcall, S. Basu, M. Pinsonneault, and A. M. Serenelli, *ibid.* **618**, 1049 (2005).
[11] Ya. B. Zel'dolvich and Yu. P. Raizer, in *Physics of Shock Waves and High Temperature Hydrodynamic Phenomena*, edited by W. D. Hayes and R. F. Probstein (Dover, Mineola, 1966).
[12] J. P. Apruzese, J. Davis, K. G. Whitney, J. W. Thornhill, P. C. Kepple, R. W. Clark, C. Deeney, C. A. Coverdale, and T. W. L. Sanford, Phys. Plasmas **9**, 2411 (2002).
[13] M. J. Seaton, Y. Yu, D. Mihalas, and A. K. Pradhan, Mon. Not. R. Astron. Soc. **266**, 805 (1994); M. J. Seaton, *ibid.* **382**, 245 (2007).
[14] C. Mendoza, M. J. Seaton, P. Buerger, A. Bellorín, M. Meléndez, J. González, L. S. Rodríguez, F. Delahaye, E. Palacios, A. K. Pradhan, and C. J. Zeippen, Mon. Not. R. Astron. Soc. **378**, 1031 (2007).
[15] D. C. Wilson, P. A. Bradley, N. M. Hoffman, F. J. Swenson, D. P. Smitherman, R. E. Chrien, R. W. Margevicius, D. J. Thoma, L. R. Foreman, J. K. Hoffer, S. R. Goldman, S. E. Caldwell, T. R. Dittrich, S. W. Haan, M. M. Marinak, S. M. Pollaine, and J. J. Sanchez, Phys. Plasmas **5**, 1953 (1998); S. W. Haan, M. C. Herrmann, T. R. Dittrich, A. J. Fetterman, M. M. Marinak, D. H. Munro, S. M. Pollaine, J. D. Salmonson, G. L. Strobel, and L. J. Suter, *ibid.* **12**, 056316 (2005).
[16] N. Grevesse and A. J. Sauval, Space Sci. Rev. **85**, 161 (1998).
[17] P. Renaudin, L. Lecherbourg, C. Blancard, P. Cosse, G. Faussurier, P. Audebert, S. Bastiani-Ceccotti, J.-P. Geindre, and R. Shepherd, AIP Conf. Proc. **926**, 24 (2007).
[18] J. J. MacFarlane, I. E. Golovkin, P. R. Woodruff, D. R. Welch, B. V. Oliver, T. A. Mehlhorn, and R. B. Campbell, *Inertial Fusion Science and Applications*, edited by B. A. Hammel, D. D. Meyerhofer, J. Meyer-ter-Vehn, and H. Azechi (American Nuclear Society, La Grange Park, 2004), p. 457; J. J. MacFarlane, I. E. Golovkin, P. Wang, P. R. Woodruff, and N. A. Pereyra, High Energy Density Phys. **3**, 181 (2007).
[19] J. E. Bailey, G. A. Rochau, C. A. Iglesias, J. Abdallah, Jr., J. J. MacFarlane, I. Golovkin, P. Wang, R. C. Mancini, P. W. Lake, T. C. Moore, M. Bump, O. Garcia, and S. Mazevet, Phys. Rev. Lett. **99**, 265002 (2007).
[20] J. E. Bailey, G. A. Rochau, R. C. Mancini, C. A. Iglesias, J. J. MacFarlane, I. E. Golovkin, J. C. Pain, F. Gilleron, C. Blancard, Ph. Cosse, G. Faussurier, G. A. Chandler, T. J. Nash, D. S. Nielsen, and P. W. Lake, Rev. Sci. Instrum. **79**, 113104 (2008).
[21] C. L. S. Lewis and J. McGlinchey, Opt. Commun. **53**, 179 (1985).
[22] T. S. Perry, S. J. Davidson, F. J. D. Serduke, D. R. Bach, C. C. Smith, J. M. Foster, R. J. Doyas, R. A. Ward, C. A. Iglesias, F. J. Rogers, J. Abdallah, Jr., R. E. Stewart, J. D. Kilkenny, and R. W. Lee, Phys. Rev. Lett. **67**, 3784 (1991).
[23] T. S. Perry, P. T. Springer, D. F. Fields, D. R. Bach, F. J. D. Serduke, C. A. Iglesias, F. J. Rogers, J. K. Nash, M. H. Chen, B. G. Wilson, W. H. Goldstein, B. Rozsynai, R. A. Ward, J. D. Kilkenny, R. Doyas, L. B. Da Silva, C. A. Back, R. Cauble, S. J. Davidson, J. M. Foster, C. C. Smith, A. Bar-Shalom, and R. W. Lee, Phys. Rev. E **54**, 5617 (1996).
[24] H. Griem, *Principles of Plasma Spectroscopy* (Cambridge University Press, New York, 1997).
[25] J. E. Bailey, G. A. Rochau, S. B. Hansen, C. A. Iglesias, J. J. MacFarlane, I. Golovkin, P. Wang, R. C. Mancini, C. Blancard, Ph. Cosse, G. Faussurier, F. Gilleron, and J. C. Pain, "Evaluation of non-LTE effects on iron plasma transmission measurements at temperatures above 150 eV," High Energy Density Phys. (to be submitted).
[26] S. J. Davidson, J. M. Foster, C. C. Smith, K. A. Warburton, and S. J. Rose, Appl. Phys. Lett. **52**, 847 (1988).
[27] J. M. Foster, D. J. Hoarty, C. C. Smith, P. A. Rosen, S. J. Davidson, S. J. Rose, T. S. Perry, and F. J. D. Serduke, Phys. Rev. Lett. **67**, 3255 (1991).
[28] J. Bruneau, C. Chenais-Popovics, D. Desenne, J.-C. Gauthier, J.-P. Geindre, M. Klapisch, J.-P. Le Breton, M. Louis-Jacquet, D. Naccache, and J.-P. Perrine, Phys. Rev. Lett. **65**, 1435 (1990).
[29] D. J. Hoarty, C. D. Bentley, B. J. B. Crowley, S. J. Davidson, S. G. Gales, P. Graham, J. W. O. Harris, C. A. Iglesias, S. F. James, and C. C. Smith, J. Quant. Spectrosc. Radiat. Transf. **99**, 283 (2006); D. J. Hoarty, J. W. O. Harris, P. Graham, S. J. Davidson, S. F. James, B. J. B. Crowley, E. L. Clark, C. C. Smith, and L. Upcraft, High Energy Density Phys. **3**, 325 (2007).
[30] J. E. Bailey, P. Arnault, T. Blenski, G. Dejonghe, O. Peyrusse, J. J. MacFarlane, R. C. Mancini, M. E. Cuneo, D. S. Nielsen, and G. A. Rochau, J. Quant. Spectrosc. Radiat. Transf. **81**, 31 (2003).
[31] C. Chenais-Popovics, F. Gilleron, M. Fajardo, H. Merdji, T. Mißalla, J. C. Gauthier, P. Renaudin, S. Gary, J. Bruneau, F. Perrot, T. Blenski, W. Fölsner, and K. Eidmann, J. Quant. Spectrosc. Radiat. Transf. **65**, 117 (2000).
[32] C. Chenais-Popovics, H. Merdji, T. Mißalla, F. Gilleron, J. C. Gauthier, T. Blenski, F. Perrot, M. Klapisch, C. Bauche-Arnoult, J. Bauche, A. Bachelier, and K. Eidmann, Astrophys. J., Suppl. Ser. **127**, 275 (2000).
[33] C. Chenais Popovics, M. Fajardo, F. Gilleron, U. Teubner, J.-C. Gauthier, C. Bauche-Arnoult, A. Bachelier, J. Bauche, T. Blenski, F. Thais, F. Perrot, A. Benuzzi, S. Turck-Chièze, J.-P. Chièze, F. Dorchies, U. Andiel, W. Foelsner, and K. Eidmann, Phys. Rev. E **65**, 016413 (2001); C. Chenais-Popovics, M. Fajardo, F. Thais, F. Gilleron, J. C. Gauthier, K. Eidmann, W. Fölsner, T. Blenski, F. Perrot, C. Bauche-Arnoult, A. Bachelier, and J. Bauche, J. Quant. Spectrosc. Radiat. Transf. **71**, 249 (2001); H. Merdji, T. Mißalla, T. Blenski, F. Perrot, J. C. Gauthier, K. Eidmann, and C. Chenais-Popovics, Phys. Rev. E **57**, 1042 (1998).
[34] C. A. Back, T. S. Perry, D. R. Bach, B. G. Wilson, C. A. Iglesias, O. L. Landen, S. J. Davidson, and B. J. B. Crowley, J. Quant. Spectrosc. Radiat. Transf. **58**, 415 (1997).
[35] F. Thais, S. Bastiani, T. Blenski, C. Chenais-Popovics, K. Eidman, W. Fölsner, J.-C. Gauthier, F. Gilleron, and M. Poirier, J. Quant. Spectrosc. Radiat. Transf. **81**, 473 (2003).
[36] P. Renaudin, C. Blancard, J. Bruneau, G. Faussurier, J.-E. Fuchs, and S. Gary, J. Quant. Spectrosc. Radiat. Transf. **99**, 511 (2006).
[37] L. Da Silva, B. J. MacGowan, D. R. Kania, B. A. Hammel, C. A. Back, E. Hsieh, R. Doyas, C. A. Iglesias, F. J. Rogers, and R. W. Lee, Phys. Rev. Lett. **69**, 438 (1992).
[38] P. T. Springer, D. J. Fields, B. G. Wilson, J. K. Nash, W. H. Goldstein, C. A. Iglesias, F. J. Rogers, J. K. Swenson, M. H. Chen, A. Bar-Shalom, and R. E. Stewart, Phys. Rev. Lett. **69**, 3735 (1992).
[39] G. Winhart, K. Eidmann, C. A. Iglesias, A. Bar-Shalom, E. Mínguez, A. Rickert, and S. J. Rose, J. Quant. Spectrosc. Radiat. Transf. **54**, 437 (1995); G. Winhart, K. Eidmann, C. A. Iglesias, and A. Bar-Shalom, Phys. Rev. E **53**, R1332 (1996).
[40] P. T. Springer, K. L. Wong, C. A. Iglesias, J. H. Hammer, J. L. Porter, A. Toor, W. H. Goldstein, B. G. Wilson, F. J. Rogers, C. Deeney, D. S. Dearborn, C. Bruns, J. Emig, and R. E. Stewart, J. Quant. Spectrosc. Radiat. Transf. **58**, 927 (1997).
[41] C. A. Iglesias and F. J. Rogers, Astrophys. J. **464**, 943 (1996).
[42] F. J. Rogers and C. A. Iglesias, Science **263**, 50 (1994).
[43] M. K. Matzen, Phys. Plasmas **4**, 1519 (1997); V. P. Smirnov, Plasma Phys. Controlled Fusion **33**, 1697 (1991); J. H. Brownell, R. L. Bowers, K. D. McLenthan, and D. L. Peterson, Phys. Plasmas **5**, 2071 (1998).
[44] J. E. Bailey, G. A. Chandler, S. A. Slutz, G. R. Bennett, G. Cooper, J. S. Lash, S. Lazier, R. Lemke, T. J. Nash, D. S. Nielsen, T. C. Moore, C. L. Ruiz, D. G. Schroen, R. Smelser, J. Torres, and R. A. Vesey, Phys. Rev. Lett. **89**, 095004 (2002); J. E. Bailey, G. A. Chandler, R. C. Mancini, S. A. Slutz, G. A. Rochau, M. Bump, T. J. Buris-Mog, G. Cooper, G. Dunham, I. Golovkin, J. D. Kilkenny, P. W. Lake, R. J. Leeper, R. Lemke, J. J. MacFarlane, T. A. Mehlhorn, T. C. Moore, T. J. Nash, A. Nikroo, D. S. Nielsen, K. L. Peterson, C. L. Ruiz, D. G. Schroen, D. Steinman, and W. Varnum, Phys. Plasmas **13**, 056301 (2006).

[45]T. W. L. Sanford, T. J. Nash, R. C. Mock, J. P. Apruzese, and D. L. Peterson, Phys. Plasmas **13**, 012701 (2006).
[46]S. A. Slutz, K. J. Peterson, R. A. Vesey, R. W. Lemke, J. E. Bailey, W. Varnum, C. L. Ruiz, G. W. Cooper, G. A. Chandler, G. A. Rochau, and T. A. Mehlhorn, Phys. Plasmas **13**, 102701 (2006).
[47]G. A. Rochau, J. E. Bailey, G. A. Chandler, G. Cooper, G. S. Dunham, P. W. Lake, R. J. Leeper, R. W. Lemke, T. A. Mehlhorn, A. Nikroo, K. J. Peterson, C. L. Ruiz, D. G. Schroen, S. A. Slutz, D. Steinman, W. A. Stygar, and W. Varnum, Plasma Phys. Controlled Fusion **49**, B591 (2007).
[48]D. D. Ryutov, M. S. Derzon, and M. K. Matzen, Rev. Mod. Phys. **72**, 167 (2000); M. K. Matzen, M. A. Sweeney, R. G. Adams, J. R. Asay, J. E. Bailey, G. R. Bennett, D. E. Bliss, D. D. Bloomquist, T. A. Brunner, R. B. Campbell, G. A. Chandler, C.A. Coverdale, M. E. Cuneo, J.-P. Davis, C. Deeney, M. P. Desjarlais, G. L. Donovan, C. J. Garasi, T. A. Haill, C. A. Hall, D. L. Hanson, M. J. Hurst, B. Jones, M. D. Knudson, R. J. Leeper, R. W. Lemke, M. G. Mazarakis, D. H. McDaniel, T. A. Mehlhorn, T. J. Nash, C. L. Olson, J. L. Porter, P. K. Rambo, S. E. Rosenthal, G. A. Rochau, L. E. Ruggles, C. L. Ruiz, T. W. L. Sanford, J. F. Seamen, D. B. Sinars, S. A. Slutz, I. C. Smith, K. W. Struve, W. A. Stygar, R. A. Vesey, E. A. Weinbrecht, D. F. Wenger, and E. P. Yu, Phys. Plasmas **12**, 055503 (2005).
[49]D. R. Kania, H. Kornblum, B. A. Hammel, J. Seely, C. Brown, U. Feldman, G. Glendinning, P. Young, E. Hsieh, M. Hennesian, L. DaSilva, B. J. MacGowan, D. S. Montgomery, C. A. Back, R. Doyas, J. Edwards, and R. W. Lee, Phys. Rev. A **46**, 7853 (1992); T. S. Perry, R. I. Klein, D. R. Bach, K. S. Budil, R. Cauble, H. N. Kornblum, Jr., R. J. Wallace, and R. W. Lee, Phys. Rev. E **58**, 3739 (1998).
[50]G. A. Rochau, J. E. Bailey, and J. J. MacFarlane, Phys. Rev. E **72**, 066405 (2005).
[51]C. Chenais-Popovics, C. Fievet, J. P. Geindre, I. Matsushima, and J. C. Gauthier, Phys. Rev. A **42**, 4788 (1990).
[52]R. F. Heeter, S. G. Anderson, R. Booth, G. V. Brown, J. Emig, S. Fulkerson, T. McCarville, D. Norman, M. B. Schneider, and B. K. F. Young, Rev. Sci. Instrum. **79**, 10E303 (2008).
[53]T. McCarville, S. Fulkerson, R. Booth, J. Emig, B. Young, S. Anderson, and B. Heeter, Rev. Sci. Instrum. **76**, 103501 (2005); S.G. Anderson, R. F. Heeter, R. Booth, J. Emig, S. Fulkerson, T. McCarville, D. Norman, and B. K. F. Young, *ibid.* **77**, 063115 (2006).
[54]B. L. Henke, F. G. Fujiwara, M. A. Tester, C. H. Dittmore, and M. A. Palmer, J. Opt. Soc. Am. B **1**, 828 (1984).
[55]B. L. Henke, J. Y. Uejio, G. F. Stone, C. H. Dittmore, and F. G. Fujiwara, J. Opt. Soc. Am. B **3**, 1540 (1986).
[56]J. E. Bailey, G. A. Chandler, D. Cohen, M. E. Cuneo, M. E. Foord, R. F. Heeter, D. Jobe, P. W. Lake, J. J. MacFarlane, T. J. Nash, D. S. Nielson, R. Smelser, and J. Torres, Phys. Plasmas **9**, 2186 (2002).
[57]N. Izumi, R. Snavely, G. Gregori, J. A. Koch, H.-S. Park, and B. A. Remington, Rev. Sci. Instrum. **77**, 10E325 (2006).
[58]C. A. Iglesias, J. Quant. Spectrosc. Radiat. Transf. **99**, 295 (2006).
[59]A. Thorne, *Spectrophysics* (Wiley, New York, 1974).
[60]M. Schneider and R. Heeter, personal communication (2008).
[61]M. C. Hermann, Bull. Am. Phys. Soc. **48**, 21 (2003); J. F. Hansen, S. G. Glendinning, R. F. Heeter, and S. J. E. Brockington, Rev. Sci. Instrum. **79**, 013504 (2008).
[62]T. S. Perry, S. J. Davidson, F. J. D. Serduke, D. R. Bach, C. C. Smith, J. M. Foster, R. J. Doyas, R. A. Ward, C. A. Iglesias, F. J. Rogers, J. Abdallah, Jr., R. E. Stewart, R. J. Wallace, J. D. Kilkenny, and R. W. Lee, Astrophys. J., Suppl. Ser. **127**, 433 (2000).
[63]A. V. Vinogradov, I. Yu. Skobelev, and E. A. Yukov, Sov. Phys. Usp. **22**, 771 (1979).
[64]M. H. Key and R.J. Hutcheon, *Advances in Atomic and Molecular Physics 16* (Academic, New York, 1980), pp. 201–280.
[65]C. De Michelis and M. Mattioli, Nucl. Fusion **21**, 677 (1981).
[66]H. R. Griem, Phys. Fluids **4**, 2346 (1992).
[67]H. R. Griem, Phys. Scr. **T83**, 142 (1999).
[68]G. Dunham, J. E. Bailey, G. A. Rochau, P. W. Lake, and L. B. Nielsen-Weber, Rev. Sci. Instrum. **78**, 063106 (2007); G. Dunham, G. A. Rochau, P. Lake, L. Nielsen-Weber, and D. Schuster, *ibid.* **75**, 3687 (2004); J.E. Bailey, R. Adams, A. L. Carlson, C. H. Ching, A. B. Filuk, and P. Lake, *ibid.* **68**, 1009 (1997).
[69]E. Nardi and Z. Zinamon, J. Appl. Phys. **52**, 7075 (1981); J. E. Bailey, J. J. MacFarlane, P. Wang, A. L. Carlson, T. A. Haill, D. J. Johnson, P. Lake, E. J. McGuire, and T. A. Mehlhorn, Phys. Rev. E **56**, 7147 (1997).
[70]J. D. Hares, J. D. Kilkenny, M. H. Key, and J. G. Lunney, Phys. Rev. Lett. **42**, 1216 (1979); A. Hauer, R. D. Cowan, B. Yaakobi, O. Barnouin, and R. Epstein, Phys. Rev. A **34**, 411 (1986).
[71]R. C. Mancini, C. F. Hooper, Jr., and R. L. Caldwell, J. Quant. Spectrosc. Radiat. Transf. **51**, 201 (1994).
[72]D. Hoarty, O. Willi, L. Barringer, C. Vickers, R. Watt, and W. Nazarov, Phys. Plasmas **6**, 2171 (1999).
[73]J. Abdallah, Jr., R. E. H. Clark, and J. M. Peek, Phys. Rev. A **44**, 4072 (1991).
[74]R. Epstein, Phys. Rev. A **43**, 961 (1991).
[75]L. Lecherbourg, P. Renaudin, S. Bastiani-Ceccotti, J.-P. Geindre, C. Blancard, P. Cosse, G. Faussurier, R. Shepherd, and P. Audebert, High Energy Density Phys. **3**, 175 (2007).
[76]L. A. Woltz and C. F. Hooper, Jr., Phys. Rev. A **38**, 4766 (1988).
[77]R. C. Mancini, D. P. Kilcrease, L. A. Woltz, and C. F. Hooper, Jr., Comput. Phys. Commun. **63**, 314 (1991).
[78]A. C. G. Mitchell and M. W. Zemansky, *Resonance Radiation and Excited Atoms* (Cambridge University Press, London, 1934).
[79]P. T. Springer, T. S. Perry, R. E. Stewart, C. A. Iglesias, F. J. Serduke, B. G. Wilson, R. W. Lee, J. M. Foster, C. C. Smith, D. J. Hoarty, and S. J. Davidson, *Proceedings of the Fourth International Workshop on Radiative Properties of Hot Dense Matter*, edited by W. Goldstein, C. Hooper, J. Gauthier, J. Seely, and R. Lee (World Scientific, River Edge, 1991), p. 42.
[80]C. A. Iglesias and F. J. Rogers, Astrophys. J. **408**, 371 (1991).